Journal of Magnetism and Magnetic Materials 361 (2014) 1–6

Contents lists available at ScienceDirect

Journal of Magnetism and Magnetic Materials

journal homepage: www.elsevier.com/locate/jmmm

Local symmetry breaking and spin–phonon coupling in $SmCrO_3$ orthochromite

M. El Amrani [a], M. Zaghrioui [a,*], V. Ta Phuoc [a], F. Gervais [a], Néstor E. Massa [b]

[a] GREMAN CNRS UMR 7347, Université F. Rabelais, IUT de Blois, 15 rue de la Chocolatrie 41029 Blois cedex, France
[b] Laboratorio Nacional de Investigacion y Servicios en Espectroscopia Optica-Centro CEQUINOR, Universidad Nacional de La Plata, C. C. 962, 1900 La Plata, Argentina

ARTICLE INFO

Article history:
Received 26 August 2013
Received in revised form
29 January 2014
Available online 24 February 2014

Keywords:
Multiferroic
Orthochromite
Raman scattering
Infrared reflectivity

ABSTRACT

Raman scattering and infrared reflectivity performed on polycrystalline $SmCrO_3$ support strong influence of the antiferromagnetic order on phonon modes. Both measurements show softening of some modes below T_N. Such a behavior is explained by spin–phonon coupling in this compound. Furthermore, temperature dependence of the infrared spectra has demonstrated important changes compared to the Raman spectra, suggesting strong structural modifications due to the cation displacements rather to those of the oxygen ions. Our results reveal that polar distortions originating in local symmetry breaking, i.e. local non-centrosymmetry, resulting in Cr off-centring.

1. Introduction

Rare earth orthochromite $RCrO_3$ (R stands for rare earth and yttrium) crystallize in an orthorhombic space group *Pnma* ($D_{2h}^{16}, Z=4$) [1] and have been subject of intense studies in the seventies because of their complex magnetic structures [2–11]. As the temperature decreases, Cr^{3+} spins become antiferromagnetically ordered at T_N (120–300 K) with a small ferromagnetic component due to the spin canting; afterward Cr^{3+} spins undergo a reorientation at T_{SR} (≤ 40 K) and at lower temperature R^{3+} spins become ordered and can be accompanied by a reorientation of Cr^{3+} spins [12–16]. Recently, weak ferroelectric behavior has been reported in this family occurring at the magnetic ordering temperature T_N making them members of multiferroic materials [17–19]. Hence a renewed interest in these compounds concerning origin of polar ordering, magnetoelectric couplings and their potential application on the development of new devices.

Orthorhombic $SmCrO_3$ is a member of the multiferroic orthochromite family, which shows anti-ferromagnetic and ferroelectric orders below $T_N=197$ K [20]. This compound presents a centric orthochromite structure at room temperature. Investigations of structural transition, versus temperature, by X-ray and neutron diffraction have shown the absence of structural phase transition below T_N [21]; and thus within this long range averaging view the space group remains unchanged even when weak ferroelectricity is detected. We then may argue that spontaneous polar order is not a long range structural change. It should be noted that the presence of ferroelectric order is not expected in centrosymmetric structure. Different explanations were then given to interpret this behavior, among them we can mention the role of exchange striction between the rare-earth moments and chromium atoms or also a local symmetry breaking due to the antiferromagnetic order [17,18,21]. However, origin and mechanism of ferroelectricity remain elusive.

The aim of this work is to study in detail the structural changes of the $SmCrO_3$ by means of Raman and infrared spectroscopies. Indeed, both probes are very sensitive to structural changes and also to local changes at very small scale. A few Raman studies have been already published on orthochromites [22,23]. However, to our knowledge, no infrared spectra have been done on these multiferroic materials. In this paper, we report for the first time infrared reflectivity measurements versus temperature on $SmCrO_3$ orthochromite. Thermal evolution of these spectra has evidenced important changes at the temperatures of magnetic transitions.

2. Experimental

Polycrystalline samples of $SmCrO_3$ were prepared by a conventional solid state reaction procedure. The oxide precursors Cr_2O_3 and Sm_2O_3 were mixed, in stoichiometric proportions (Sm:Cr=1:1 ratio), in ethanol. After alcohol evaporation, the mixture was

* Corresponding author. Tel.: +33 255542105.
E-mail address: zaghrioui@univ-tours.fr (M. Zaghrioui).

http://dx.doi.org/10.1016/j.jmmm.2014.02.057
0304-8853

compacted and calcined, in a box furnace, at 1200 °C for 12 h. X-ray diffraction diagram, made after a grinding step, on the obtained powders confirmed the formation of the orthochromite $SmCrO_3$ phase. Thereafter the powders were pelletized and sintered in air at 1400 °C for 12 h [24] in order to obtain dense pellets required for infrared reflectivity measurements. X-ray diffraction diagram (XRD) was obtained at room temperature in the angular range from 10° to 80°, with a step size of 0.02° using a Bruker D8 diffractometer operating with CuK_α radiation. Lattice parameters were calculated by Full-profile matching using FULL-PROF program and the Rietveld method [25,26]. Chemical composition was controlled with an energy-dispersive X-ray (EDS) detector, coupled at a scanning electron microscope. The cationic ratio, Sm/Cr=0.98, determined by the EDS analysis is close to the nominal one. Magnetic properties of the polycrystalline samples were measured over the temperature range 5–300 K in an applied field of 1 kOe under both zero field cooling (ZFC) and field cooling (FC) conditions, using the VSM option in the QD-PPMS device. Raman spectra were collected, between 80 and 300 K, using a Renishaw Invia Reflex and a commercial temperature control stage (Linkam THMS600). The excitation wavelength of 514.5 nm was used, with a power less than 1 mW focused on the sample. An objective L × 50 magnification was used to focus the laser beam and to collect the scattered light dispersed by a holographic grating of 2400 lines per mm. Near normal incidence infrared reflectivity spectra were measured with a Bruker IFS 66 v/S in the wavenumber range of 50–8000 cm^{-1} and versus temperature from 10 up to 300 K. A layer of gold was applied on the sample in situ and reassessed based on the temperature. These data were used as a reference to calculate mirror reflectivity to take into account the scattering of light on the sample surface.

3. Results and discussions

3.1. Powder X-ray diffraction and magnetic susceptibility

XRD diagram collected at room temperature is shown in Fig. 1. It confirms the formation of $SmCrO_3$ single phase crystallized in orthorhombic structure in agreement with results reported in the literature [1]. Moreover, no impurity or secondary phases were detected in the limit of the device resolution. All observed peaks are well indexed in orthorhombic structure with space group *Pnma* as demonstrated by the Rietveld refinement in Fig. 1. Cell parameters deduced from refinement analysis (a=5.4983(2),

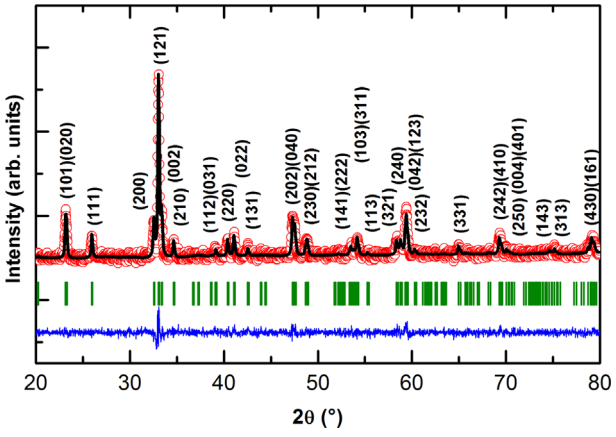

Fig. 1. Observed and calculated X-ray diffraction patterns at room temperature. The difference between the observed and calculated patterns is plotted at the bottom and the Bragg reflections are drawn as streak marks between both.

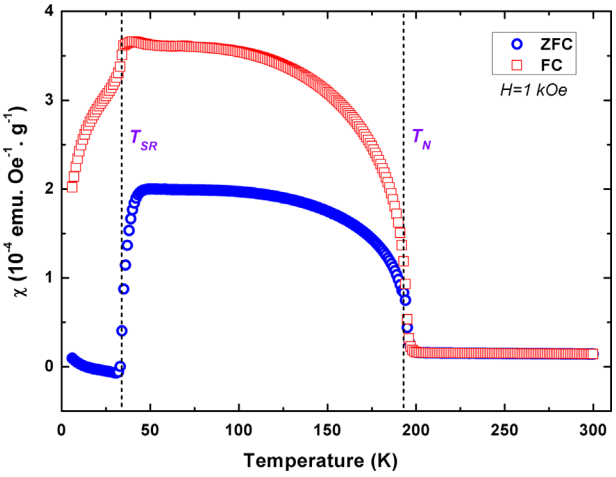

Fig. 2. Temperature variation of the zero field cooled and field cooled magnetization at an applied field of 1000 Oe.

b=7.6442(3) and c=5.3668(2) Å) are also in agreement with those reported by other authors [1,27].

Fig. 2 shows the magnetic susceptibilities versus temperature obtained in ZFC and FC conditions under an applied field of 1 kOe. ZFC and FC curves present two magnetic transitions at T_N=197 K and T_{SR}=34 K, which correspond to paramagnetic–antiferromagnetic and spin reorientation transitions, respectively [27,28]. At T_N chromium spins order antiferromagnetically and adopt the configuration $\Gamma_4(G_x, A_y, F_z)$ following the Bertaut notation [2,29]. This mode leads to the appearance of weak ferromagnetic component along the z axis, which explains the bifurcation between ZFC and FC curves below T_N (Fig. 2). At T_{SR}, Cr spin configuration changes to $\Gamma_2(F_x, C_y, G_z)$, reflecting magnetic anisotropy interactions between Sm and Cr ions [17]. Both XRD and magnetization analyses indicate the high quality of our samples.

3.2. Raman scattering

Raman spectra, versus temperature, recorded in backscattering configuration are plotted in Fig. 3. All spectra are normalized with respect to the uppermost band and a linear baseline has already been subtracted to take into account the background contribution. Raman spectrum at room temperature is similar to that obtained by Weber et al. and Bhadram et al. [22,23] and shows 16 phonon modes over 24 modes expected from the group theory ($7A_g+5B_{1g}+7B_{2g}+5B_{3g}$) [30,31]. Phonon modes were assigned according to results reported by Iliev et al. [31] and Weber et al. [22] on $RCrO_3$ (R=La, Y) single crystals and $RCrO_3$ (R=Y, La, Pr, Sm, Gd, Dy, Ho, Yb, Lu) polycrystalline compounds.

The temperature dependence of spectra, shown in Fig. 3, presents slight changes. The number of phonon modes remains unchanged between 80 and 300 K, implying that no structural transition occurring at T_N. Otherwise, phonon mode frequencies present different behaviors as illustrated in Fig. 4a. Some modes exhibit a standard temperature dependence, while others show an anomaly around T_N. The same description can be done for the linewidth temperature dependence (Fig. 4b).

As a general rule, the temperature dependent of phonon mode frequency $\omega(T)$ is due to the change of the lattice volume $\Delta\omega_{latt}$, the intrinsic anharmonic contribution $\Delta\omega_{anh}$, the spin–lattice coupling $\Delta\omega_{s-p}$ and the electron–phonon coupling $\Delta\omega_{e-p}$ [34,23]:

$$\omega(T) = \omega_0 + \Delta\omega_{latt}(T) + \Delta\omega_{anh}(T) + \Delta\omega_{e-p} + \Delta\omega_{s-p}(T)$$

ω_0 corresponds to the frequency at 0 K. As a rough approximation electron–phonon coupling can be neglected, for $SmCrO_3$, because

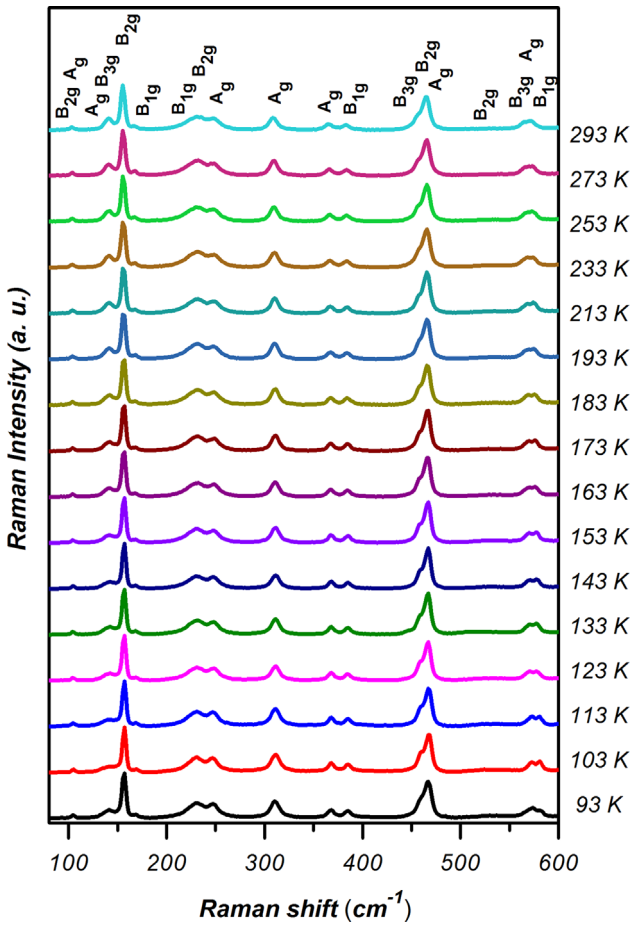

Fig. 3. Raman spectra of $SmCrO_3$ compound versus temperature measured with 514 nm excitation.

of the low carrier concentration. The intrinsic anharmonic contribution corresponds to the frequency shift at constant volume and reads as

$$\Delta\omega_{anh}(T) = -C[1+2/(e^{\hbar\omega_0/kT}-1)]$$

where C is a fit parameter. According to the plot of phonon frequencies and line width versus temperature: (i) B_{2g}^1 mode exhibits a standard temperature dependence due to the anharmonic effect; (ii) B_{2g}^2 mode presents hardening below T_N due to the magnetostriction effect and this is consistent with its line width variation [23]; (iii) A_g^1 and A_g^2 modes slightly soften below T_N, which could be related to a spin–phonon coupling as demonstrated by the plot of their line width versus temperature [23]. Indeed, such a behavior could not be explained by the change of the cell volume. Thermal frequency evolution indicates thus the frequency shift is mainly due to the anharmonic contribution and the spin–phonon coupling, other effects could be neglected. Note that these results are in good agreement with those reported by Bhadram et al., which also have led to the same conclusions [23].

3.3. Infrared reflectivity

Fig. 5 shows variation with temperature between 13 and 300 K of the infrared reflectivity spectra of $SmCrO_3$, in the phonon modes frequency range. The spectrum at room temperature is a characteristic of distorted perovskite and can be divided into four regions [32,33]: (i) region 1 (100–250 cm^{-1}) corresponds to external modes where Sm sub-lattice moves against the CrO sub-lattice; (ii) region 2 (250–350 cm^{-1}) corresponds to oxygen displacements. These modes originate from T_{2u} silent mode in cubic perovskite, and they become active due to the symmetry reduction; (iii) region 3 (350–550 cm^{-1}) corresponds to bending modes O–Cr–O within octahedra and (iv) region 4 (550–700 cm^{-1}) corresponds to stretching modes involving Cr and O displacements. All these phonon modes are originating from the center of Brillouin zone and from zone boundaries (R, X and M) of cubic perovskite in $Pm3m$ space group.

At 300 K, at least 18 modes can be identified over 25 expected modes from the group theory ($9B_{1u}+7B_{2u}+9B_{3u}$) for orthorhombic $SmCrO_3$ with $Pnma$ space group.

In contrast to the thermal dependence of the Raman spectra, the thermal evolution of reflectivity spectra is more important. What strongly suggests that cations are responsible of these infrared changes rather than the anions, since Raman active phonons of $SmCrO_3$ mainly involve oxygen atoms. Moreover, significant changes are observed in the vicinity of the magnetic temperatures transitions (T_{SR} and T_N) implying pronounced effect of magnetic orders. These changes occur mainly in the regions of external modes (region 1) and the O–Cr–O bending modes (region 3) as indicated by arrows in Fig. 5. More precisely, new phonon modes appears below T_N around 144 , 160 and 370 cm^{-1}. The first two modes are external and correspond to the rare earth beating against octahedra in the SmO_{12} cages. This may suggest a non-negligible role for Sm as known for the rare earth buckling in the ferroelectric transition in hexagonal manganites [35]. In addition, the three phonons located between 400 and 450 cm^{-1} also undergo significant changes. At room temperature, the three modes are well separated and well resolved; whereas below T_N they merge to form a broad band. The changes in region 3 suggest changes in Cr–O bond distances, O–Cr–O angles and/or tilt of CrO_6 octahedra. The new phonons in region 1 can be related to the antiferromagnetic order and spin reorientation of Cr spins, i.e. the new magnetic structure reduces the symmetry leading the appearance of the new modes at 144 cm^{-1} and 160 cm^{-1}. All the observed changes, in infrared spectra, clearly indicate that the cations are subject to significant displacements in the vicinity of the magnetic transition.

In order to follow thermal evolution of phonon mode frequency, Kramers–Kroning transformation of reflectivity spectra was performed. Imaginary part of dielectric function (ϵ) obtained by this procedure is shown in Fig. 6; where the main changes are indicated by arrows. The plot of ω_{TO} (T) of some selected modes is shown in Fig. 7. With decreasing temperature some mode frequencies decrease, while others increase. However, all show anomaly at about T_N indicating that the antiferromagnetic order, of Cr^{3+} spins, affects the phonon frequencies.

Note that, as shown in Fig. 7b, an anomaly is observed around 140 K (noted $T^\star$) for some infrared and Raman modes and could be connected to the maximum of χT product occurring at the same temperature. This anomaly was also reported by Bhadram et al. for certain Raman modes of $SmCrO_3$ and was attributed to precursors of the spin-reorientation transition [23].

Let us focus on external modes (region 1). Two new phonon modes are observed below T_N. The first mode, located at 160 cm^{-1} (called below SR-mode), becomes clearly visible below 100 K and the second mode, at 144 cm^{-1} (AFM-mode), appears at T_N. The thermal evolution of their ω_{TO} is shown in Fig. 8a. ω_{TO} of the SR-mode increases between 100 and 40 K, presents a jump between 40 and 30 K and then saturates. Behavior of this mode clearly shows spin reorientation transition occurring at 34 K as was observed in magnetization measurements. ω_{TO} of the AFM-mode decreases with decreasing temperature. This mode softens by 10% between 200 and 13 K and its temperature dependence can be associated with magnetic ordering. As discussed in the previous

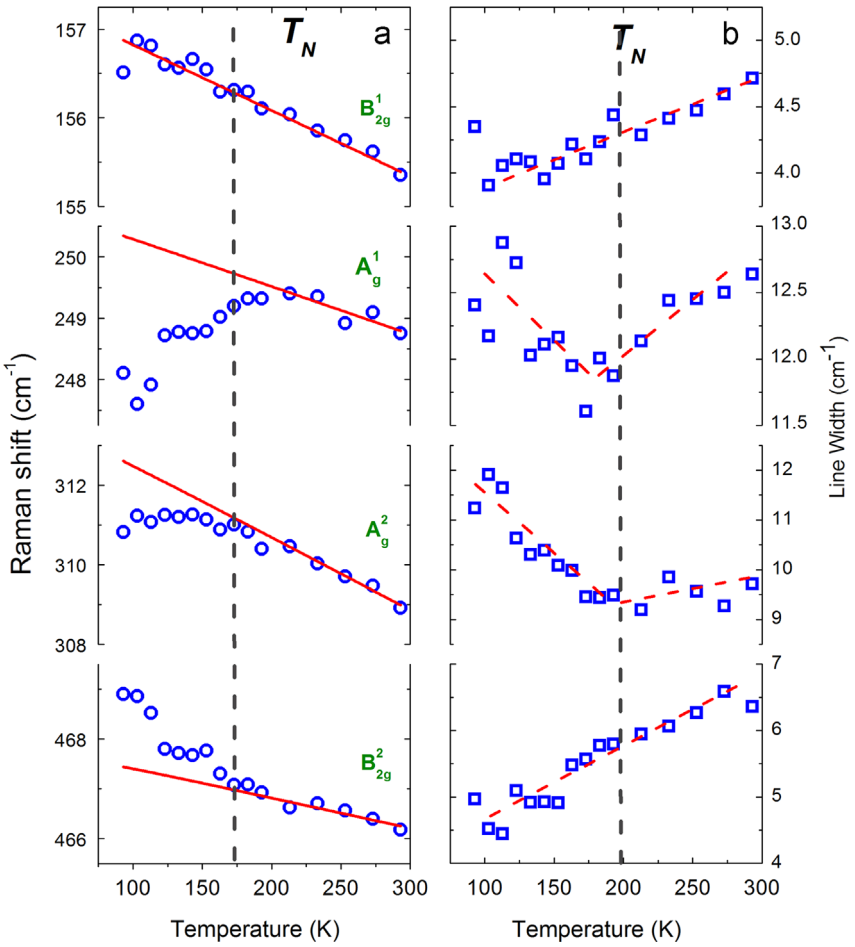

Fig. 4. Evolution of Raman shift (left panel) and line width (right panel) versus temperature for some selected Raman modes. Solid lines correspond to the temperature dependence of frequency for anharmonic phonon–phonon scattering. Dashed lines are guide for the eye.

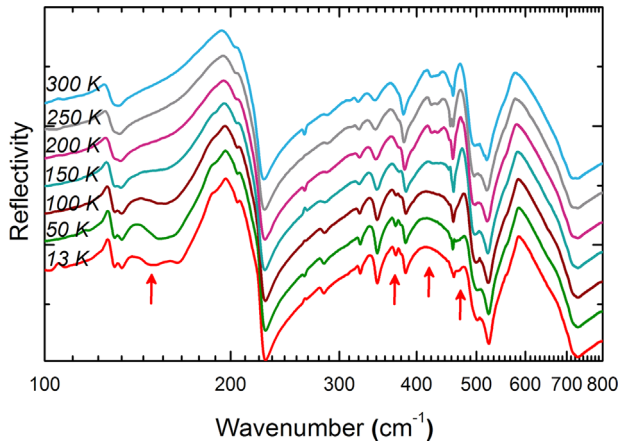

Fig. 5. Infrared reflectivity spectra of polycrystalline $SmCrO_3$ as a function of temperature. Arrows indicate the main changes.

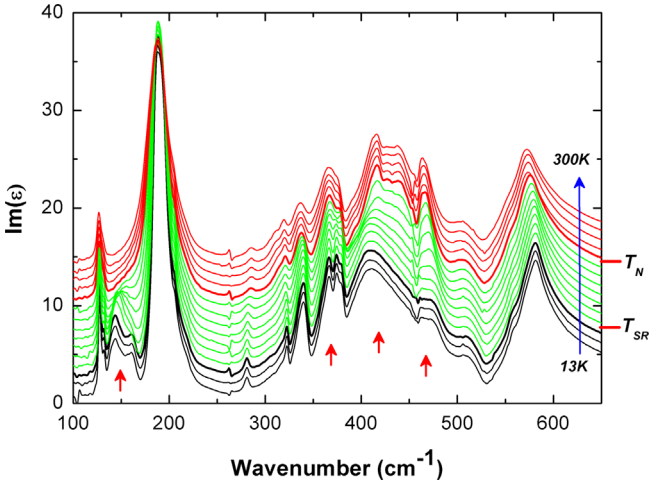

Fig. 6. Thermal dependence of imaginary part of the dielectric function between 13 and 300 K.

section, the frequency change versus temperature is mainly due to the intrinsic anharmonic contribution and the spin–phonon coupling. In addition, in the case of magnetic materials, the frequency renormalization $\Delta\omega_{s-p}$ corresponds to the phonon modulation of exchange coupling constant and is proportional to spin–spin correlation function $\langle S_i.S_j\rangle$ for the nearest-neighbor (NN) spins [34,36]:

$$\Delta\omega_{s-p} = \omega_{TO}(T) - \omega_0 - \Delta\omega_{anh}(T) = \lambda < S_i.S_j > (T) \quad (1)$$

where λ is the spin–phonon coupling coefficient. The spin–spin correlation function can be described by mean field theory by the normalized order parameter, hence the temperature dependence of the frequency mode can be written as follows:

$$\omega_{TO}(T) = \omega_0 + \Delta\omega_{anh}(T) - \lambda S^2[1-(T/T_N)^{\gamma}] \quad (2)$$

The modelization of $\omega_{TO}(T)$ of AFM-mode, using Eq. 4, was performed by fixing T_N and S to 197 K and 3/2, respectively.

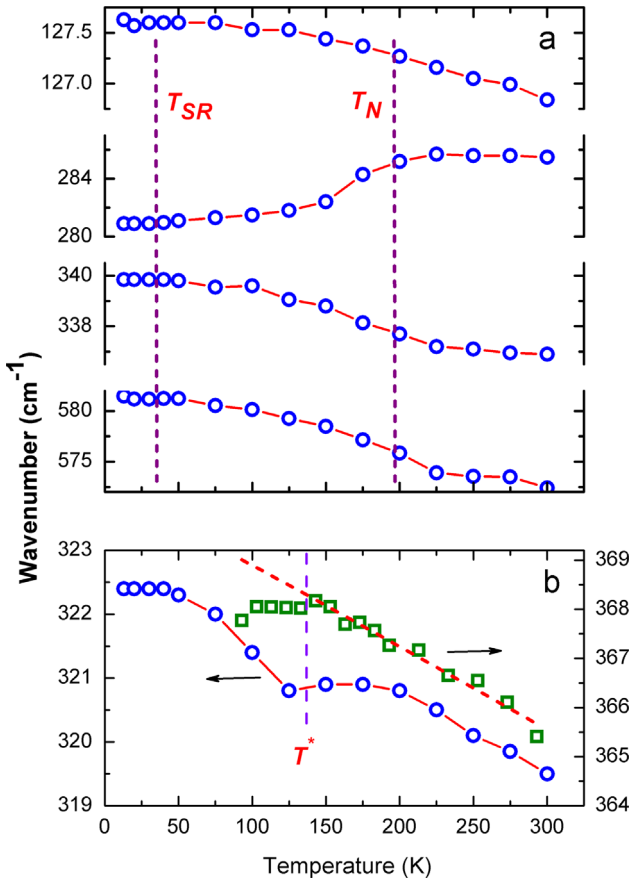

Fig. 7. (a) Temperature dependence of TO frequencies of selected infrared active modes of $SmCrO_3$ compound. (b) Thermal evolution of Raman (square) and IR (circle) mode frequencies showing anomaly at T^*.

In addition, $\omega_{anh}(T)$ was assumed to be temperature independent $\approx\omega_0$ because of the lack of data above T_N. As shown in Fig. 8a (solid line), $\omega_{TO}(T)$ dependence is well described by spin–phonon coupling. The best fit is obtained for $\omega_0 = 160\ \mathrm{cm}^{-1}$, $\lambda = 7.8(3)\ \mathrm{cm}^{-1}$ and $\gamma = 1.5(2)$. λ is higher than that found in antiferromagnetic materials, which indicates a large spin–phonon coupling in orthochromite $SmCrO_3$ compound. Nevertheless, this value is in the same order than was reported for Cr_2O_3 [37]. Otherwise, the same treatment was done for another phonon mode, located at 281 cm^{-1}, which also softens below T_N. Temperature dependence is also well described by spin–phonon coupling model as shown in Fig. 8b. However, λ and γ values are different from those of the AFM-mode, particularly spin–phonon coefficient which is smaller than for the previous mode. This can be explained by the fact that both modes involve different atoms and displacements. This also indicates that the AFM-mode is more sensitive to magnetic orders and more particularly to the interaction between magnetic rare earth and chromium; because this mode involves the movement of Sm sub-lattice against CrO sublattice. These interpretations are supported by the comparison of frequency renormalization of both infrared modes and magnetization. Indeed, $\omega_{TO}(T)$ of the high frequency mode scales as M^2, which is not the case for the AFM-mode as shown in Fig. 9. The high frequency mode has the same behavior versus temperature than phonon modes affected by spin–phonon coupling in orthorhombic $RMnO_3$ and ordered double perovskite(La_2CoMnO_6 and La_2NiMnO_6) [34,36,38–40]. The frequency shift of this mode is then described by only coupling between NN Cr^{3+} spins. However, the magnetic interactions between Sm–Cr and next-nearest-neighbor (NNN) Cr^{3+} spins cannot be neglected for the AFM-mode.

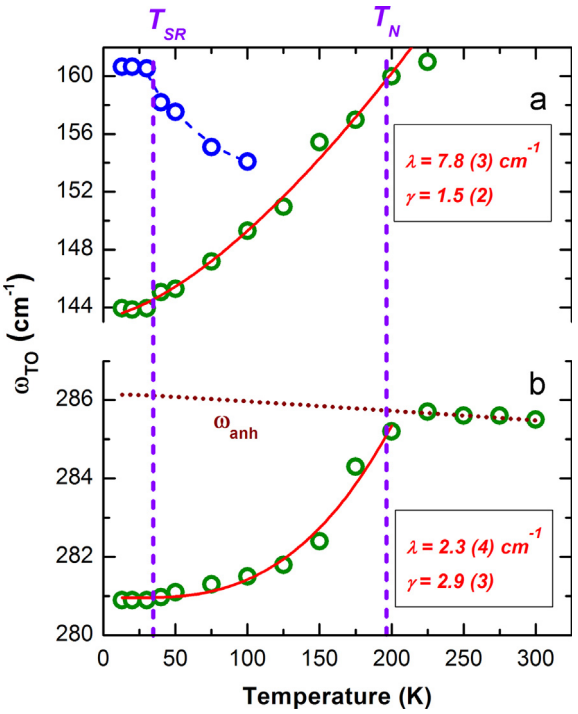

Fig. 8. Temperature dependence of infrared active modes observed at (a) low frequency below T_N and (b) high frequency. Solid lines correspond to the fit using spin–phon coupling model and dashed line is guide for the eye.

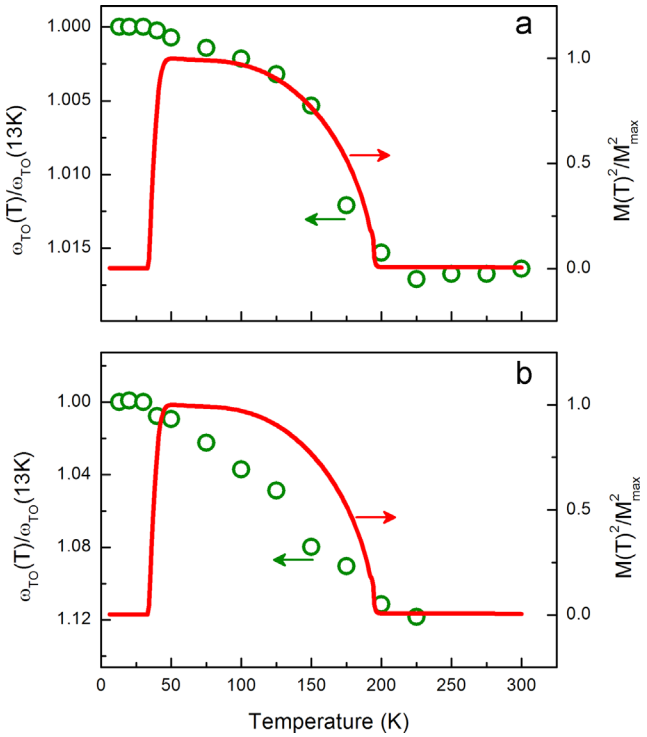

Fig. 9. Temperature dependence of the frequency shift of the 281 cm^{-1} (a) and the 144 cm^{-1} (b) modes. Solid lines correspond to the square of the experimental magnetization.

Our results clearly indicate strong distortion of the lattice below T_N. Indeed, apparition of new polar modes and softening of some optical modes can be related to the lifting of degeneracy (modes splitting), probably resulting in the motion of the cations from their equilibrium position (centers of polyhedra CrO_6 and

SmO_{12}). The fact that infrared phonon modes at the region 3 undergo significant changes allows one to suspect that Cr^{3+} ions move from the octahedron center and reduce the symmetry leading to the apparition of ferroelectric order. This displacement can cause either symmetry breaking locally or more generally a structural transition. In the latter case, the new structure should be non-centrosymmetric and derived from the high temperature structure because of the similarity between reflectivity and Raman spectra below and above T_N. The subgroups that satisfy these criteria are $Pna2_1$, $Pmn2_1$ and $Pmc2_1$, which are polar. In such a case, all IR active modes also become Raman active, which is invalidated by our results. That leads to a suggestion that ferroelectricity in $SmCrO_3$ is most probably due to a local symmetry breaking resulting in off-centering of chromium ions in CrO_6 octahedron, in accordance with the 0.1 Å displacement of Cr^{3+} ions measured by high resolution neutron diffraction in $YCrO_3$ [21]. In addition, Cr–Sm magnetic interactions must play an important role in this mechanism because of the significant changes occurring in external mode region in IR spectra. Consequently, exchange striction of Cr–Sm exchange and local symmetry breaking would contribute to the establishment of ferroelectric polarization below T_N.

4. Conclusion

We have investigated Raman and far infrared spectra of the multiferroic $SmCrO_3$ versus temperature. Our results show clearly interplay between magnetism and lattice. Some Raman and infrared active modes present softening in the antiferromagnetic phase, which was described by spin–phonon coupling. More interestingly, infrared spectra show strong lattice distortion below T_N. Apparition of new modes below this temperature and significant changes in phonon spectra reflect the influence of magnetic order. In addition, the interpretation of these observations allows us to suppose that the ferroelectricity in $SmCrO_3$ is the consequence of cation movements from their central position in oxygen polyhedra.

References

[1] S. Geller, Acta Cryst. 10 (1957) 243–248.
[2] G. Gorodetsky, R.M. Hornreich, S. Shaft, B. Sharon, A. Shaulov, B.M. Wanklyn, Phys. Rev. B 16 (1977) 515–521.
[3] R.M. Hornreich, S. Shtrikman, B.M. Wanklyn, I. Yaeger, Phys. Rev. B 13 (1976) 4046–4052.
[4] J.D. Gordon, R.M. Hornreich, S. Shtrikman, B.M. Wanklyn, Phys. Rev. B 13 (1976) 3012–3017.
[5] A. Hasson, R.M. Hornreich, Y. Komet, B.M. Wanklyn, I. Yaeger, Phys. Rev. B 12 (1975) 5051–5067.
[6] I.S. Jacobs, F. Hugh, L. Burne, M. Levinson, J. Appl. Phys. 42 (1971) 11631–11632.
[7] K. Tsushima, K. Aoyagi, S. Sugano, J. Appl. Phys. 41 (1970) 1238–1240.
[8] P. Pataud, J. Sivardiere, J. Phys. Fr. 31 (1970) 803–809.
[9] R.M. Hornreich, Y. Komet, R. Nolan, B.M. Wanklyn, I. Yaeger, Phys. Rev. B 12 (1975) 5094–5104.
[10] R.S. Meltzer, Phys. Rev. B 2 (1970) 2398–2411.
[11] J.P. van der Ziel, L.G. Van Uitert, J. Appl. Phys. 40 (1969) 997–998.
[12] H.B. Lal, K. Kaur, R.D. Dwivedi, J. Mater. Sci. Lett. 14 (1995) 9–11.
[13] K. Sardar, M.R. Lees, R.J. Kashtiban, J. Sloan, R.I. Walton, Chem. Mater. 23 (2011) 48.
[14] N. Shamir, H. Shaked, S. Shtrikman, Phys. Rev. B 24 (1981) 6642.
[15] K. Yoshii, J. Solid State Chem. 159 (2001) 204.
[16] C. Moure, O. Pena, J. Magn. Magn. Mater. 337 (2013) 1060.
[17] B. Rajeswaran, D.I. Khomskii, A.K. Zvezdin, C.N.R. Rao, A. Sundaresan, Phys. Rev. B 86 (2012) 214409.
[18] Claudy Rayan Serrao, Asish K. Kundu, S.B. Krupanidhi, Umesh V. Waghmar, C.N.R. Rao, Phys. Rev. B 72 (2005) 220101.
[19] Jyoti Ranjan Sahu, Claudy Rayan Serrao, Nirat Ray, Umesh V. Waghmare, C.N.R. Rao, J. Mater. Chem. 17 (2007) 42–44.
[20] J.-S. Zhou, J.A. Alonso, V. Pomjakushin, J.B. Goodenough, Y. Ren, J.-Q. Yan, J.-G. Cheng, Phys. Rev. B 81 (2010) 214115.
[21] K. Ramesha, A. Llobet, Th. Proffen, C.R. Serrao, C.N.R. Rao, J. Phys.: Condens. Matter 19 (2007) 102202.
[22] M.C. Weber, J. Kreisel, P.A. Thomas, M. Newton, K. Sardar, R.I. Walton, Phys. Rev. B 85 (2012) 054303.
[23] Venkata Srinu Bhadram, B. Rajeswaran, A. Sundaresan, Chandrabhas Narayana, Eur. Phys. Lett. 101 (2013) 17008.
[24] A.K. Tripathi, H.B. Lal, J. Mater. Sci. 17 (1982) 1595–1609.
[25] H.M. Rietveld, Acta Cryst. 22 (1967) 151–152.
[26] J. Rodriguez-Carvajal, T. Roisnel, Commission for powder diffraction, Int. Union Crystallogr. Newsl. 20 (1998).
[27] Kripasindhu Sardar, Martin R. Lees, Reza J. Kashtiban, Jeremy Sloan, Richard I. Walton, Chem. Mater. 23 (2011) 48–56.
[28] T. Yamaguchi, J. Phys. Chem. Solids 35 (1974) 479–500.
[29] E.F. Bertaut, G. Bassi, G. Buisson, P. Burlet, J. Chappert, A. Delapalme, J. Mareschal, G. Roult, R. Aleonard, R. Pauthenet, J.P. Rebouillat, J. Appl. Phys. 37 (1966) 1038–1039.
[30] M. Udagawa, K. Kohn, N. Koshizuka, T. Tsushima, K. Tsushima, Solid Stat. Commun. 16 (1975) 779–783.
[31] M.N. Iliev, A.P. Litvinchuk, V.G. Hadjiev, Y.-Q. Wang, J. Cmaidalka, R.-L. Meng, Y.-Y. Sun, N. Kolev, M.V. Abrashev, Phys. Rev. B 74 (2006) 214301.
[32] Ph. Ghosez, E. Cockayne, U.V. Waghmare, K.M. Rabe, Phys. Rev. B 60 (1999) 836.
[33] V. Zelezny, E. Cockayne, J. Petzelt, M.F. Limonov, D.E. Usvyat, V.V. Lemanov, A.A. Volkov, Phys. Rev. B 66 (2002) 224303.
[34] E. Granado, A. García, J.A. Sanjurjo, C. Rettori, I. Torriani, F. Prado, R.D. Sánchez, A. Caneiro, S.B. Oseroff, Phys. Rev. B 60 (1999) 11879–11882.
[35] Bas B. Van Aken, Jan-Willem G. Bos, Robert A. de Groot, Thomas T.M. Palstra, Phys. Rev. B 63 (2001) 125127.
[36] J. Laverdière, S. Jandl, A.A. Mukhin, V.Yu. Ivanov, V.G. Ivanov, M.N. Iliev, Phys. Rev. B 73 (2006) 214301.
[37] C.H. Hung, P.H. Shih, F.Y. Wu, W.H. Li, S.Y. Wu, T.S. Chan, H.S. Sheu, J. Nanosci. Nanotechnol. 10 (2010) 4596–4601.
[38] W. Kaczmarek, I. Mrke, J. Magn. Magn. Mater. 58 (1986) 91–96.
[39] M.N. Iliev, M.V. Abrashev, A.P. Litvinchuk, V.G. Hadjiev, H. Guo, A. Gupta, Phys. Rev. B 75 (2007) 104118.
[40] M.N. Iliev, H. Guo, A. Gupta, Appl. Phys. Lett. 90 (2007) 151914.